Laser diode nonlinear dynamics from a filtered phase-conjugate optical feedback

Lionel Weicker,[1,*] Thomas Erneux,[2] Delphine Wolfersberger,[1] and Marc Sciamanna[1]
[1]*OPTEL Research Group, CentraleSupélec, LMOPS (EA 4423), 2 rue Édouard Belin, 57070 Metz, France*
[2]*Optique Nonlinéaire Théorique, Université Libre de Bruxelles, Campus Plaine, CP 231, 1050 Bruxelles, Belgium*
(Received 12 April 2015; published 12 August 2015)

The rate equations for a laser diode subject to a filtered phase-conjugate optical feedback are studied both analytically and numerically. We determine the Hopf bifurcation conditions, which we explore by using asymptotic methods. Numerical simulations of the laser rate equations indicate that different pulsating intensity regimes observed for a wide filter progressively disappear as the filter width increases. We explain this phenomenon by studying the coalescence of Hopf bifurcation points as the filter width increases. Specifically, we observe a restabilization of the steady-state solution for moderate width of the filter. Above a critical width, an isolated bubble of time-periodic intensity solutions bounded by two successive Hopf bifurcation points appears in the bifurcation diagram. In the limit of a narrow filter, we then demonstrate that only two Hopf bifurcations from a stable steady state are possible. These two Hopf bifurcations are the Hopf bifurcations of a laser subject to an injected signal and for zero detuning.

DOI: 10.1103/PhysRevE.92.022906 PACS number(s): 05.45.−a, 42.60.Rn, 02.30.Ks

I. INTRODUCTION

Semiconductor lasers subject to different optical feedbacks have attracted much interest during the last 40 years. First as a laboratory tool to explore nonlinear dynamics of systems with time delay [1], and second for their potential to drive applications based on chaos [2]. Such feedbacks can be achieved, for example, from an external mirror [3–5], from an optoelectronic feedback [6–8], from polarization-rotated optical feedback [9–13], or from phase-conjugate feedback (PCF) [14–18]. As the light is reflected back to the laser cavity, it modifies drastically the laser output. In order to investigate theoretically the different behaviors, the starting point is often based on modified Lang-Kobayashi equations [3]. These equations are delay differential equations (DDEs) and the resulting dynamics depends on several parameters, such as the laser injection current, the reflectivity of the external mirror, and the length of the external cavity.

Recently, PCF has attracted a lot of attention. Dedicated new experiments identified several features not present in conventional optical feedback, including superharmonic self-pulsating solutions and high-frequency harmonic pulsing dynamics underlying chaotic low-frequency fluctuations. Simulations of the PCF laser equations have shown a rich variety of dynamics. Depending on the feedback strength, steady-state solution [19], external-cavity-modes (ECMs) [19,20], chaos [21], low-frequency fluctuation (LFF) [22,23], extreme events [24], and undamped oscillations with frequency close to the laser relaxation frequency [25] can be observed. Of particular physical interest are the ECMs that have been investigated both theoretically [17,19,20] and experimentally [26]. In the PCF configuration, ECMs are defined as self-pulsating intensity solutions with a period close to an integer multiple of the external-cavity round-trip time. It has been shown that ECMs emerge from Hopf bifurcations [19,20]. From the ECM limit-cycle solutions, LFFs emerge through secondary bifurcations [23]. Whereas in general the finite-penetration-depth phase-conjugate mirror (PCM) is neglected, few studies take it into account. In 1998, a rate equation model was proposed in order to explore its effect [27]. The authors observed that a long PCM tends to filter out high frequencies. This suggests that the ECMs might disappear for long PCMs. Among the different investigations of this model, a theoretical study on the stability of the steady states has been realized for discrete values of the finite-penetration depth [28]. The authors have shown that for finite values of the depth PCM, restabilization of the steady-state solution is possible. On the other hand, Green *et al.* [29,30] studied numerically this problem using a continuation method. They proposed different bifurcation scenarios as function of the pump parameter and the feedback strength for discrete values of the finite-penetration-depth. The system is described mathematically as a laser diode subject to a delayed filtered phase-conjugate feedback (FPCF).

In this paper, we formulate dimensionless equations for the FPCF. We determine analytic expressions of the Hopf bifurcation conditions. Based on numerical simulations, we show that the different ECMs observed for a zero-penetration-depth PCM disappear as the penetration depth increases. Using the Hopf bifurcation conditions, we explain this phenomenon by noting successive coalescence of Hopf bifurcation points as the depth increases. Another phenomenon is also observed: for a range of finite penetration depth, a restabilization of the steady-state solution can be achieved between two critical values of the feedback strength. A further increase of the feedback strength above the second critical value leads to successively destabilizing and stabilizing Hopf bifurcations of our basic steady state, hence forming a bubble of time-periodic oscillating intensity dynamics. This bubble is explained by our analysis of the Hopf bifurcation points. It leads to a range of the feedback strength where the response of the laser is steady between different oscillatory regimes. This range depends on the finite penetration depth. We also demonstrate that for a narrow filter (or very long PCM), only three Hopf bifurcations exist. The first and the last ones are responsible for the destabilization and restabilization of the steady state. These bifurcations are reachable experimentally for low and moderate feedbacks and are matching the Hopf bifurcation

*lionel.weicker@centralesupelec.fr

points of a laser subject to an injected signal and for zero detuning.

The organization of the paper is as follows. In Sec. II, we introduce a dimensionless model describing a semiconductor laser subject to a feedback from a finite-penetration-depth phase-conjugate mirror. In Sec. III, we investigate numerically different bifurcation diagrams for different values of the penetration time τ_r. In Sec. IV, we study the seven first Hopf bifurcations in order to explain the disappearance of the ECMs when the finite depth increases. From this analysis, we also identify the bifurcation mechanism leading to the bubble of periodic oscillations. We then provide asymptotic expressions for the different Hopf bifurcations for large finite-depth PCM in Sec. V. Finally, we summarize our main results in Sec. VI.

II. FORMULATION

A semiconductor laser subject to a feedback from a finite-interaction-depth PCM can be described by the following dimensionless rate equations

$$\frac{dY}{dt} = (1 + i\alpha)YZ + \gamma U, \tag{1}$$

$$T\frac{dZ}{dt} = P - Z - (1 + 2Z)|Y|^2, \tag{2}$$

$$\frac{dU}{dt} = \frac{1}{\tau_r}[Y^*(t - \tau) - U], \tag{3}$$

where $Y(t)$ corresponds to the complex electric field, $U(t)$ is the complex feedback field, and $Z(t)$ represents the carrier density. In order to obtain these equations, we have followed the approximations of Ref. [27] where the frequency dependence of the PCM reflectivity has been neglected. See Appendix A for details about the formulation of these equations. γ represents the dimensionless feedback rate and is mathematically defined as

$$\gamma = \tau_p'\kappa = \tau_p'\frac{(1 - R_m)}{\tau'}\sqrt{\frac{\eta_c R_{PCM}}{R_m}}, \tag{4}$$

where η_c is the coupling efficiency, R_m the laser facet reflectivity, R_{PCM} the reflectivity of the PCM, τ_p' the photon lifetime, and τ' the external cavity round-trip time. α corresponds to the linewidth enhancement factor, τ is the external cavity round-trip time normalized by the photon lifetime, T is defined as the ratio of the carrier and photon lifetimes, τ_r corresponds approximately to the time the light takes to penetrate the PCM normalized by the photon lifetime, P is the pump parameter above threshold, and t is the dimensionless time. In several previous theoretical studies [19,20,29], the following set of parameter values is considered

$$\alpha = 3, \quad \tau = 476, \quad T = 1428, \quad P = 0.0417. \tag{5}$$

These values are typical of a semiconductor laser subject to a 10-cm-distant mirror feedback and working close to threshold. The multiple delayed round trips in the extended cavity are not taken into account in this model since we are interested in relatively low reflectivities of the external mirror. If $\tau_r \to 0$, Eqs. (1)–(3) reduce to the equations of a PCF with a zero-penetration-depth PCM. We note that this model also corresponds mathematically to a semiconductor laser subject to a filtered phase-conjugate feedback in which the mirror penetration time τ_r would play the role of the inverse of the filter bandwidth. In this context, we are interested to study the case of a narrow filter ($\tau_r \to \infty$).

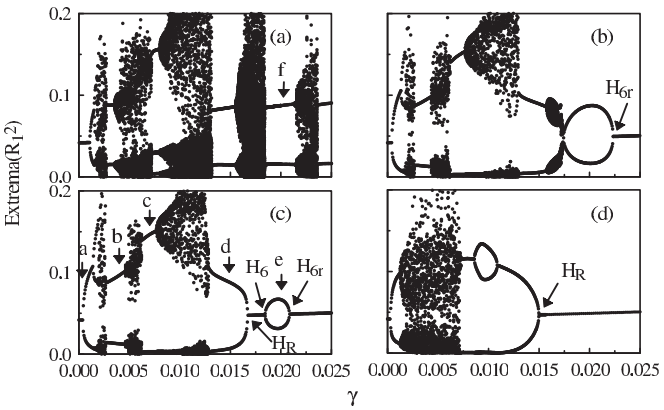

FIG. 1. Bifurcation diagrams corresponding to the extrema of the output intensity R_1^2 with γ as the bifurcation parameter. The different bifurcation diagrams have been obtained from Eqs. (B1)–(B5). (a) for $\tau_r = 1$, (b) for $\tau_r = 100$, (c) for $\tau_r = 115$, (d) for $\tau_r = 1000$. The values of the parameters are fixed to $P = 0.0417$, $\tau = 476$, $T = 1428$, and $\alpha = 3$. The time series at the letters a-f are represented in Figs. 2(a)–2(f), respectively.

III. NUMERICAL RESULTS

In order to explore the effects of the penetration-depth PCM (or equivalently the effects of the filter width of a FPCF) on the dynamics of the laser, we propose different bifurcation diagrams for different values of τ_r with γ as the bifurcation parameter, see Fig. 1. γ has been chosen as our bifurcation parameter because it is experimentally tunable through a variable attenuator.

For low values of τ_r, we observe similar behaviors as in the case of a zero-depth PCM. See Fig. 1(a) for the case $\tau_r = 1$. For low feedback rate, a Hopf bifurcation leading to relaxation oscillations of frequency close to the laser relaxation frequency emerges from the steady-state solution. Increasing the feedback leads to a cascade of different oscillatory regimes (period-doubling, chaos, etc.). For higher values of the feedback rate, different external cavity modes (ECMs) are observed.

If we increase τ_r by two orders of magnitude, the dynamics is very different. No more ECMs are observed and the range of feedback strength corresponding to chaos decreases. See Fig. 1(b) for $\tau_r = 100$. Of particular interest is the bubble of oscillatory dynamics that appears between $\gamma \simeq 0.0172$ and $\gamma \simeq 0.0215$, and the steady state, which restabilizes at H_{6r}.

Increasing slightly τ_r leads to a region of restabilization of the steady state between two oscillatory states. See Fig. 1(c) for $\tau_r = 115$. We observe the destabilizations and restabilizations of the steady state at $\gamma \simeq 3 \times 10^{-4}$ (which corresponds to H_1 in the next section), $\gamma \simeq 0.0167$ (H_R), $\gamma \simeq 0.0184$ (H_6), and $\gamma \simeq 0.0208$ (H_{6r}). The resulting bubble of time-periodic dynamics exists for a smaller range of the feedback strength but is isolated between two stable steady states. Increasing τ_r

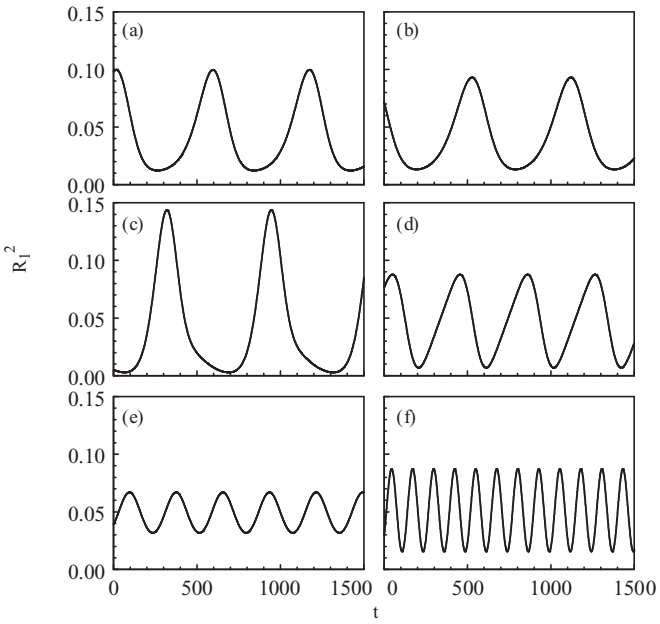

FIG. 2. Different time series of the output intensity. (a)–(f) correspond to the letters a–f in Figs. 1(a) and 1(b). (a) $\gamma = 0.000438$, $\tau_r = 115$, (b) $\gamma = 0.00356$, $\tau_r = 115$, (c) $\gamma = 0.006688$, $\tau_r = 115$, (d) $\gamma = 0.015$, $\tau_r = 115$, (e) $\gamma = 0.02$, $\tau_r = 115$, and (f) $\gamma = 0.02$, $\tau_r = 1$. The values of the other parameters are the same as in Fig. 1.

reduces the interval of feedback strength values that separates H_6 and H_{6r}. When $\tau_r \gtrsim 121$, this bubble disappears.

Figure 1(d) corresponds to $\tau_r = 1000$. The bifurcation diagram again changes drastically. There is no bubble of time-periodic oscillations anymore and the interval of feedback strength leading to chaotic dynamics is again smaller. Moreover, the system exhibits a stable steady state for either low or high feedback rate, i.e., when the feedback rate is set outside two values. As τ_r increases, we note that the destabilization and restabilization of the steady state tend to occur at approximately fixed values of γ, i.e., $\gamma \simeq 3 \times 10^{-4}$ (which corresponds to H_1 in the next section) and $\gamma \simeq 0.0157$ (H_R).

Different time series corresponding to different periodic regimes are represented in Fig. 2. Figures 2(a)–2(e) are obtained for $\gamma = 0.000438$, $\gamma = 0.00356$, $\gamma = 0.006688$, $\gamma = 0.015$, and $\gamma = 0.02$, respectively, when $\tau_r = 115$. For Figs. 2(a)–2(d), we note that the shape and the period of the solutions change with the feedback strength. From previous studies on the PCF system, we know that the frequencies of the dynamics, Figs. 2(a)–2(c), are related to the laser relaxation frequency.

Figure 2(e) corresponds to a periodic solution in the bubble of oscillatory dynamics. The period is close to 280. In order to know if the period in this area is related to the external cavity round trip, we tried to find the bubble of oscillations for very different values of the delay. We noted that changing the delay modifies both the range of feedback strength and the range of τ_r where the bubble of oscillations can be observed. However, it does not significantly influence the frequency of the oscillations inside the bubble. For example, if we fix $\tau = 800$, the bubble exists between $\tau_r \simeq 134$ and $\tau_r \simeq 163$. For $\tau_r = 150$, the period of the oscillations is close to 299. In all cases, this dynamics disappears for large τ_r as evidenced in Fig. 1(d). Indeed, as it will be described in detail in Sec. V, this limit corresponds to a system with optical injection with zero detuning—a situation in which the steady state destabilizes and restabilizes through undamped relaxation oscillations.

ECMs in the PCF laser system are defined as oscillations of the intensity at frequency being a harmonic of the external cavity frequency. Figure 2(f) is an example of ECM observed in our system for $\tau_r = 1$. The period of the solution is close to $\tau/4$, which typically corresponds to an ECM (fourth harmonic).

As seen in Ref. [28], restabilization of the steady state can be obtained when the penetration depth is not zero. However, the bubble of periodic oscillations between two stable steady states was not identified. In Sec. IV, we explore this phenomenon by investigating the seven first Hopf bifurcations as functions of τ_r and γ. From this analysis, we also explain the disappearance of the ECMs as τ_r increases.

IV. HOPF BIFURCATIONS

Equations (1)–(3) admit three steady-state solutions: the trivial steady state $(Y,Z,U) = (0,P,0)$, and two distinct branches of nonsymmetric steady states given by Eqs. (B6)–(B8) in Appendix B.

The conditions for a Hopf bifurcation are given by Eqs. (B10) and (B11) where C and σ represent the amplitude of Z and the frequency of the oscillations at the Hopf bifurcation point, respectively. If we consider a zero-penetration-depth PCM ($\tau_r = 0$), these conditions reduce to the one derived in Ref. [19].

Based on the numerical observations, we study the first Hopf bifurcations when τ_r increases. To this end, we use the Newton-Raphson method applied to the Hopf conditions (B10) and (B11) in order to find the different Hopf branches. As initial values of C and σ, we consider the values referenced in Ref. [19] for $\tau_r = 0$. We then follow the different solutions by increasing τ_r, see Fig. 3(a). Figure 3(b) is a blow up of Fig. 3(a) for low values of τ_r.

From the seven first Hopf bifurcations, only two (H_1 and H_4) exist for $\tau_r \geqslant 121$. The other bifurcations coalesce with other Hopf bifurcations at critical values of τ_r. See, for example, H_6, which coalesces with H_{6r} at $\tau_r \simeq 121$. H_R is another Hopf bifurcation that also exists for higher values of the penetration-depth PCM. This Hopf bifurcation has been obtained with the help of the asymptotic analysis developed in Sec. V. Previous studies have shown that the ECMs emerge from Hopf bifurcations but, as it will be demonstrated in Sec. V, only three Hopf bifurcations (H_1, H_4, and H_R) exist for high values of τ_r. Specifically, we note that the Hopf bifurcation points γ corresponding to H_1, H_4, and H_R tend to three distinct values as τ_r increases. They do not depend on the delay, which implies that they cannot lead to ECMs. The Hopf bifurcation frequencies are represented in Fig. 3(c). Figure 3(d) is a blow up of Fig. 3(c) for low values of τ_r. We note that H_1 always destabilizes the steady state and if τ_r is large, the steady state is restabilized through H_R.

For intermediate values of τ_r (between $\tau_r = 100$ and 121), the situation is slightly different. H_R still restabilizes the steady

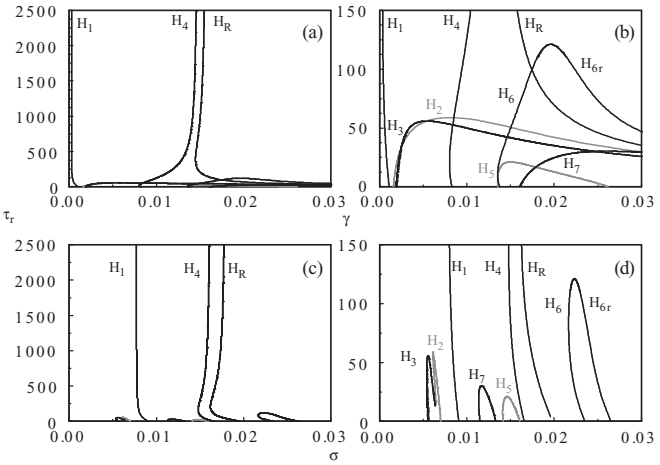

FIG. 3. Different Hopf bifurcations in the parameter plans (γ,τ_r) [(a) and (b)], and (σ,τ_r) [(c) and (d)]. The different branches of Hopf bifurcations have been obtained using the Newton-Raphson method applied to the Hopf conditions (B10) and (B11). For the H_i where $i = 1,\ldots,7$, we used the values of C and σ found in Ref. [19] as our initial conditions and followed the different branches by increasing τ_r. H_R has been obtained using the approximations (10) and (11) obtained in Sec. V as initial conditions for $\tau_r = 2500$ and then decreasing τ_r to zero. (b) and (d) are blow ups of (a) and (c), respectively. The values of the parameters are $P = 0.0417$, $\alpha = 3$, $T = 1428$, and $\tau = 476$.

state but it becomes again unstable at H_6. It leads to a range of γ where the steady state is stable between H_R and H_6. The bubble of oscillations observed in Figs. 1(b) and 1(c) for $\tau_r = 100$ and 115 emerges from H_6 and ends at H_{6r}. The steady state then restabilizes at H_{6r}. These results are in perfect agreement with numerical simulations. Since H_6 and H_{6r} exist up to $\tau_r \simeq 121$, the bubble of oscillations exists between $\tau_r \simeq 100$ and 121 for our values of parameters.

V. ASYMPTOTIC ANALYSIS OF THE HOPF BIFURCATIONS FOR LARGE VALUES OF τ_r

If τ_r is large, we can simplify Eqs. (B10) and (B11). Assuming all other parameters fixed, the leading contributions of Eqs. (B10) and (B11) are $O(\tau_r^2)$ and are given by

$$\sigma^2 = C^2(1+\alpha^2) - \varepsilon\frac{1+2P}{1+2C}2C + 2\varepsilon(P-C), \tag{6}$$

$$0 = C^3(1+\alpha^2) - \varepsilon\frac{1+2P}{1+2C}2C^2 + \varepsilon(P-C)C(1-\alpha^2) + \varepsilon^2\frac{1+2P}{1+2C}\left[\frac{1+2P}{1+2C}C - (P-C)\right], \tag{7}$$

where $\varepsilon \equiv 1/T$. Equations (6) and (7) admit three solutions for $P = 0.0417$:

$$C = -9.5183\times10^{-5};\quad \sigma = 7.6663\times10^{-3};$$
$$\gamma = 3.0099\times10^{-4},$$
$$C = 4.6699\times10^{-3};\quad \sigma = 1.6215\times10^{-2};$$
$$\gamma = 1.4768\times10^{-2},$$

TABLE I. Hopf bifurcations points and frequencies for large τ_r

γ_{analytic}	γ_{numeric}	σ_{analytic}	σ_{numeric}
2.9990×10^{-4}	3.0099×10^{-4}	7.6422×10^{-3}	7.6663×10^{-3}
1.5284×10^{-2}	1.5757×10^{-2}	1.7088×10^{-2}	1.7925×10^{-2}

$$C = -4.9827\times10^{-3};\quad \sigma = 1.7925\times10^{-2};$$
$$\gamma = 1.5757\times10^{-2},$$

where $\gamma = |C|\sqrt{1+\alpha^2}$. This relation has been obtained from Eqs. (B6) and (B7). The first and the last Hopf bifurcations are listed in Table I. From Eqs. (6) and (7), we note that the Hopf bifurcations for τ_r large do not depend on the delay. We next look for asymptotic solutions of the first and last Hopf bifurcations in the limit $\varepsilon \to 0$ and for $\alpha > 1$. We first consider the low feedback case corresponding to the first Hopf bifurcation. From our numerical results, we assume the following scalings

$$P = O(1),\quad C = O(\varepsilon),\quad \tau = O(\varepsilon^{-1}),$$
$$\tau_r \geqslant O\left(\varepsilon^{-2}\right),\quad \sigma = O(\varepsilon^{1/2}).$$

We then collect the leading terms in Eqs. (B10) and (B11) and obtain

$$\sigma = \sqrt{2\varepsilon P}, \tag{8}$$

$$C = \frac{\varepsilon(1+2P)}{1-\alpha^2}. \tag{9}$$

The values of γ and σ with $P = 0.0417$ are listed in Table I.

Second, we consider the moderate feedback case, which corresponds to the last Hopf bifurcation. From our numerical results, we assume the following approximations

$$P = O(1),\quad C = O(\varepsilon^{1/2}),\quad \tau = O(\varepsilon^{-1}),$$
$$\tau_r \geqslant O(\varepsilon^{-2}),\quad \sigma = O(\varepsilon^{1/2}),$$

and obtain from Eqs. (B10) and (B11) the leading approximations

$$C^2 = \frac{\varepsilon P(\alpha^2-1)}{1+\alpha^2}, \tag{10}$$

$$\sigma^2 = \varepsilon P(1+\alpha^2). \tag{11}$$

The values of γ and σ with $P = 0.0417$ are listed in Table I.

The expressions of the two Hopf bifurcation points and their frequencies are exactly matching the expressions found for the two Hopf bifurcations of the laser subject to an injected signal with zero detuning [31]. Physically, the relaxation of the filter feedback field becomes extremely slow in the limit of a narrow filter ($\tau_r/\tau \to \infty$). Its evolution on the long time then depends on the fast time average of the laser field as

$$\frac{dU}{dt} = \frac{1}{\tau_r}\left[-U + \lim_{t\to\infty}\frac{1}{t}\int_0^t Y^*(t'-\tau)dt'\right].$$

See Appendix C for details.

VI. CONCLUSIONS

In this paper, we explore the bifurcation possibilities of a semiconductor laser subject to a feedback from a finite-penetration-depth phase-conjugate mirror (PCM). The laser is described mathematically by the equations of a semiconductor laser subject to a filtered phase-conjugate feedback (FPCF). Few theoretical studies have been done and, to the best of our knowledge, no experimental investigations have been realized to account for the impact of the filter width on the laser dynamics. Depending on the filter width and using the feedback strength as bifurcation parameter, we predict three very different dynamical scenarios.

At low penetration depth of the PCM, or equivalently for an unbound filter width, the system acts like a laser subject to a feedback from a zero-penetration-depth PCM. ECMs are observed but disappear progressively as the penetration depth of the PCM increases. We explain this phenomenon by the coalescence of different Hopf bifurcations at critical values of the penetration depth of the PCM.

At moderate penetration depth of the PCM, or moderate filter width, the steady-state solution can be found as stable for up to three different ranges of the feedback strength. Particularly interesting is an isolated bubble of periodic solutions, which appears in the bifurcation diagram. This bubble exists in a range of feedback strength where the steady state is unstable and emerges from two stable steady states through two Hopf bifurcations. The range of feedback strength of the bubble can be increased or decreased by varying the penetration depth of the PCM.

For a narrow filter, or equivalently very large (up to infinite) penetration-depth PCM, the system admits three Hopf bifurcations. The first and the last ones are responsible for the destabilization and restabilization of the steady-state solution. We show that these two bifurcations are the Hopf bifurcation points of a laser subject to injection and for zero detuning. The problem in the limit of a narrow filter is similar to an injection laser problem where the effect of the delayed feedback is averaged on the long time scale of the relaxation.

The transition from a delayed-feedback regime to an injection regime occurs roughly when $\tau_r > 150$. The penetration time relates to the interaction length $L \cong \frac{\tau_r \tau_p c}{n}$ where n is the medium refractive index. If, for example, we consider a PR crystal for building the PCM through a transmission grating [26], this means a crystal length of approximatively $L/2 = 1.16$cm ($n = 2.7$). This is therefore a physically attainable value close to the one of the experimental setup in Ref. [26]. It also means that the observation of the bubble of oscillations is experimentally possible for realistic values of the interaction length.

ACKNOWLEDGMENTS

L.W., D.W., and M.S. acknowledge the Conseil Régional de Lorraine, FEDER through the project PHOTON, and the Agence Nationale de la Recherche (ANR) TINO project (ANR-12-JS03-005). T.E. is grateful of the support of the F.N.R.S. This work also benefited from the support of the Belgian Science Policy Office under Grant No IAP-7/35 photonics@be.

APPENDIX A: DIMENSIONLESS EQUATIONS

The rate equations describing a laser diode subject to a feedback from a finite-penetration-depth PCM referenced in Ref. [27] can be rewritten as

$$\frac{dE}{dt'} = \frac{1}{2}\left[G_N(N-N_0) - \frac{1}{\tau_p'}\right](1+i\alpha)E + \kappa F, \tag{A1}$$

$$\frac{dN}{dt'} = \frac{I}{q} - \frac{N}{\tau_e'} - G_N(N-N_0)|E|^2, \tag{A2}$$

$$\frac{dF}{dt'} = \frac{1}{\tau_r'}[E^*(t'-\tau') - F], \tag{A3}$$

where we assumed no nonlinear gain saturation and the phase detuning $\delta_0 = 0$. $E(t')$ corresponds to the slowly varying complex electric field, $N(t')$ is the population inversion number, and $F(t')$ corresponds to the complex feedback field. The meaning of the different parameters is listed in Table II. We introduce the following new variables

$$t \equiv t'/\tau_p', Y \equiv \sqrt{\frac{\tau_e' G_N}{2}}E,$$

$$Z \equiv \frac{G_N \tau_p'}{2}\left(N - N_0 - \frac{1}{G_N \tau_p'}\right), \quad U \equiv \sqrt{\frac{\tau_e' G_N}{2}}F$$

into Eqs. (A1)–(A3) and obtain

$$\frac{dY}{dt} = (1+i\alpha)YZ + \gamma U, \tag{A4}$$

$$T\frac{dZ}{dt} = P - Z - (1+2Z)|Y|^2, \tag{A5}$$

$$\frac{dU}{dt} = \frac{1}{\tau_r}[Y^*(t-\tau) - U], \tag{A6}$$

where

$$\gamma = \kappa\tau_p', \quad \tau = \tau'/\tau_p', \quad \tau_r = \tau_r'/\tau_p', \quad T = \tau_e'/\tau_p',$$

$$I_{\text{th}} = \frac{N_{\text{sol}} q}{\tau_e'}, \quad N_{\text{sol}} = N_0 + \frac{1}{G_N \tau_p'},$$

$$P = \frac{G_N \tau_p' N_{\text{sol}}}{2}\left(\frac{I - I_{\text{th}}}{I_{\text{th}}}\right).$$

TABLE II. Meaning of the parameters of the model equations (A1)–(A3).

Parameter	Meaning
G_N	Optical gain
N_0	Transparency electron number
τ_p'	Photon lifetime
α	Linewidth enhancement factor
κ	Feedback rate
I	Pump current
q	Electron charge
τ_e'	Electron lifetime
τ_r'	Time the light takes to penetrate the PCM
τ'	External cavity round-trip time

APPENDIX B: STEADY STATES AND HOPF BIFURCATION CONDITIONS

The trivial steady state is $(Y,Z,U) = (0,P,0)$. In order to find the other steady states, we introduce the phase-amplitude decompositions

$$Y = R_1 \exp(i\varphi_1), \quad U = R_2 \exp(i\varphi_2)$$

into Eqs. (A4)–(A6), we obtain

$$\frac{dR_1}{dt} = R_1 Z + \gamma R_2 \cos(\varphi_2 - \varphi_1), \tag{B1}$$

$$\frac{d\varphi_1}{dt} = \alpha Z + \gamma \frac{R_2}{R_1} \sin(\varphi_2 - \varphi_1), \tag{B2}$$

$$T\frac{dZ}{dt} = P - Z - (1+2Z)R_1^2, \tag{B3}$$

$$\frac{dR_2}{dt} = \frac{1}{\tau_r}\{R_1(t-\tau)\cos[\varphi_1(t-\tau)+\varphi_2] - R_2\}, \tag{B4}$$

$$\frac{d\varphi_2}{dt} = -\frac{1}{\tau_r}\frac{R_1(t-\tau)}{R_2}\sin[\varphi_1(t-\tau)+\varphi_2]. \tag{B5}$$

The conditions $R_1' = R_2' = \varphi_1' = \varphi_2' = Z' = 0$ lead to the steady-state solutions, i.e., two branches of solutions for Z given by

$$2\varphi_1 = -\arctan(\alpha), \quad Z = C = \frac{-\gamma}{\sqrt{1+\alpha^2}}, \tag{B6}$$

$$2\varphi_1 = \pi - \arctan(\alpha), \quad Z = C = \frac{\gamma}{\sqrt{1+\alpha^2}}, \tag{B7}$$

where

$$\varphi_1 = -\varphi_2, \quad R_1^2 = \frac{P-C}{1+2C} > 0, \quad R_1 = R_2. \tag{B8}$$

The steady-state solutions are the same as in the case of a zero-depth PCM [19] except that $\varphi_1 = -\varphi_2$ and $R_1 = R_2$. From the linearized equations, we determine the characteristic equation for the growth rate λ of a small perturbation

$$\begin{aligned} 0 = {} & (1+\tau_r\lambda)(P-C)2\varepsilon \\ & \times \{C(1+\alpha^2)[(1+\tau_r\lambda)+\exp(-\lambda\tau)] - \lambda(1+\tau_r\lambda)\} \\ & + [\exp(-2\lambda\tau) - (1+\tau_r\lambda)^2]\left(\frac{1+2P}{1+2C}\varepsilon + \lambda\right)C^2(1+\alpha^2) \\ & + (2C\lambda - \lambda^2)(1+\tau_r\lambda)^2\left(\frac{1+2P}{1+2C}\varepsilon + \lambda\right), \end{aligned} \tag{B9}$$

where $\varepsilon \equiv 1/T$. Looking for real eigenvalues and assuming $\lambda = O(|C|) \to 0$ as $|C| \to 0$, we find $\lambda = 2C(1+\alpha^2)$ in first approximation. Therefore only the branch $C < 0$ is stable as γ increases from zero. We then wonder if a Hopf bifurcation may destabilize the steady state. To this end, we introduce $\lambda = i\sigma$ into Eq. (B9). Separating the real and imaginary parts, we obtain the following two equations for C and σ

$$\begin{aligned} 0 = {} & 2\varepsilon(P-C)\{C(1+\alpha^2)[1+\cos(\sigma\tau) - \tau_r^2\sigma^2 + \tau_r\sigma\sin(\sigma\tau)] + 2\tau_r\sigma^2\} \\ & + \varepsilon\frac{1+2P}{1+2C}\{[\cos(2\sigma\tau) - 1 + \tau_r^2\sigma^2]C^2(1+\alpha^2) + \sigma^2 - \tau_r^2\sigma^4 - 4\sigma^2 C\tau_r\} \\ & + \sigma\{C^2(1+\alpha^2)[\sin(2\sigma\tau) + 2\tau_r\sigma] - 2\tau_r\sigma^3 - 2C\sigma(1-\tau_r^2\sigma^2)\}, \end{aligned} \tag{B10}$$

$$\begin{aligned} 0 = {} & 2\varepsilon(P-C)\{C(1+\alpha^2)[2\tau_r\sigma - \sin(\sigma\tau) + \tau_r\sigma\cos(\sigma\tau)] - \sigma + \tau_r^2\sigma^3\} \\ & + \varepsilon\frac{1+2P}{1+2C}\{-C^2(1+\alpha^2)[\sin(2\sigma\tau) + 2\tau_r\sigma] + 2C\sigma - 2C\tau_r^2\sigma^3 + \sigma^3 2\tau_r\} \\ & + \sigma\{C^2(1+\alpha^2)[\cos(2\sigma\tau) - 1 + \tau_r^2\sigma^2] + \sigma^2(1-4C\tau_r) - \tau_r^2\sigma^4\}. \end{aligned} \tag{B11}$$

APPENDIX C: ANALYSIS IN THE LIMIT $\tau_r/\tau \to \infty$

We introduce

$$s = t/\tau, \quad Z = \tau^{-1}z, \quad \gamma = \tau^{-1}\eta$$

into Eqs. (A4)–(A6), which leads to

$$\frac{dY}{ds} = (1+i\alpha)Yz + \eta U, \tag{C1}$$

$$T\tau^{-2}\frac{dz}{ds} = P - |Y|^2 - \tau^{-1}z(1+2|Y|^2), \tag{C2}$$

$$\frac{dU}{ds} = \varepsilon'[Y^*(s-1) - U], \tag{C3}$$

where $\varepsilon' \equiv \tau/\tau_r$. We now consider U as slowly relaxing, which leads us to develop Y, z, and U as

$$Y = Y_0(s,\upsilon) + \varepsilon' Y_1(s,\upsilon) + \ldots, \tag{C4}$$

$$z = z_0(s,\upsilon) + \varepsilon' z_1(s,\upsilon) + \ldots, \tag{C5}$$

$$U = U_0(s,\upsilon) + \varepsilon' U_1(s,\upsilon) + \ldots, \tag{C6}$$

where $\upsilon \equiv \varepsilon' s = t/\tau_r$. The leading problem if $\varepsilon' \to 0$ is given by

$$\begin{aligned} Y_{0s} &= (1+i\alpha)Y_0 z_0 + \eta U_0, \\ T\tau^{-2}z_{0s} &= P - |Y_0|^2 - \tau^{-1}z_0(1+2|Y_0|^2), \\ U_{0s} &= 0, \end{aligned}$$

which implies

$$U_0 = U_0(\upsilon).$$

The $O(\varepsilon')$ problem for U_1 reads as

$$U_{1s} = -U_{0\upsilon} + [Y_0^*(s-1) - U_0],$$

which requires the following solvability condition

$$\frac{dU_0}{d\upsilon} = -U_0 + \lim_{s\to\infty} \frac{1}{s} \int_0^s Y_0^*(s'-1)ds'.$$

The problem then becomes similar to an injection laser problem where the effect of the delayed feedback is averaged on the long time scale of the relaxation.

[1] M. C. Soriano, J. García-Ojalvo, C. R. Mirasso, and I. Fischer, Rev. Mod. Phys. **85**, 421 (2013).
[2] M. Sciamanna and K. A. Shore, Nature Photon. **9**, 151 (2015).
[3] R. Lang and K. Kobayashi, IEEE J. Quantum Electron. **16**, 347 (1980).
[4] G. Van Tartwijk, A. Levine, and D. Lenstra, IEEE J. Sel. Top. Quantum Electron. **1**, 466 (1995).
[5] G. H. M. van Tartwijk and D. Lenstra, Quantum Semiclassical Opt. **7**, 87 (1995).
[6] H. Abarbanel, M. Kennel, L. Illing, S. Tang, H. Chen, and J. Liu, IEEE J. Quantum Electron. **37**, 1301 (2001).
[7] F. Y. Lin and J. M. Liu, Opt. Commun. **221**, 173 (2003).
[8] C.-H. Lee and S.-Y. Shin, Appl. Phys. Lett. **62**, 922 (1993).
[9] T. Heil, A. Uchida, P. Davis, and T. Aida, Phys. Rev. A **68**, 033811 (2003).
[10] D. W. Sukow, K. L. Blackburn, A. R. Spain, K. J. Babcock, J. V. Bennett, and A. Gavrielides, Opt. Lett. **29**, 2393 (2004).
[11] G. Friart, L. Weicker, J. Danckaert, and T. Erneux, Opt. Express **22**, 6905 (2014).
[12] N. Oliver, M. C. Soriano, D. W. Sukow, and I. Fischer, Opt. Lett. **36**, 4632 (2011).
[13] M. Sciamanna, T. Erneux, F. Rogister, O. Deparis, P. Mégret, and M. Blondel, Phys. Rev. A **65**, 041801 (2002).
[14] A. Murakami, J. Ohtsubo, and Y. Liu, IEEE J. Quantum Electron. **33**, 1825 (1997).
[15] A. Murakami and J. Ohtsubo, IEEE J. Quantum Electron. **34**, 1979 (1998).
[16] G. P. Agrawal and G. R. Gray, Phys. Rev. A **46**, 5890 (1992).
[17] B. Krauskopf, G. R. Gray, and D. Lenstra, Phys. Rev. E **58**, 7190 (1998).
[18] A. Murakami and J. Ohtsubo, Opt. Rev. **6**, 359 (1999).
[19] T. Erneux, A. Gavrielides, K. Green, and B. Krauskopf, Phys. Rev. E **68**, 066205 (2003).
[20] M. Virte, A. Karsaklian Dal Bosco, D. Wolfersberger, and M. Sciamanna, Phys. Rev. A **84**, 043836 (2011).
[21] G. R. Gray, D. Huang, and G. P. Agrawal, Phys. Rev. A **49**, 2096 (1994).
[22] A. K. Dal Bosco, D. Wolfersberger, and M. Sciamanna, Europhys. Lett. **101**, 24001 (2013).
[23] É. Mercier, D. Wolfersberger, and M. Sciamanna, Opt. Lett. **39**, 4021 (2014).
[24] A. Karsaklian Dal Bosco, D. Wolfersberger, and M. Sciamanna, Opt. Lett. **38**, 703 (2013).
[25] G. H. M. van Tartwijk, H. J. C. van der Linden, and D. Lenstra, Opt. Lett. **17**, 1590 (1992).
[26] A. K. Dal Bosco, D. Wolfersberger, and M. Sciamanna, Appl. Phys. Lett. **105**, 081101 (2014).
[27] D. H. DeTienne, G. R. Gray, G. P. Agrawal, and D. Lenstra, IEEE J. Quantum Electron. **33**, 838 (1997).
[28] W. A. van der Graaf, L. Pesquera, and D. Lenstra, Opt. Lett. **23**, 256 (1998).
[29] K. Green and B. Krauskopf, Phys. Rev. E **66**, 016220 (2002).
[30] K. Green and B. Krauskopf, Opt. Commun. **231**, 383 (2004).
[31] T. Erneux and P. Glorieux, *Laser dynamics* (Cambridge University Press, Cambridge, 2010).